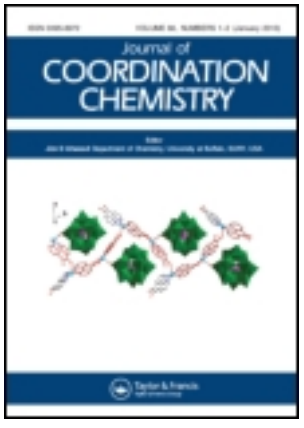

Journal of Coordination Chemistry
Publication details, including instructions for authors and subscription information:
http://www.tandfonline.com/loi/gcoo20

Synthesis, crystal structure, and properties of two metal complexes of imidazole and an ONO donor hydrazone

Fengying Chen [a b], Zhenguo Jin [b], Hengxin Li [a] & Shuiyang He [a]
[a] College of Chemistry and Material Science, Shaanxi Key Laboratory of Physical-Inorganic Chemistry, Northwest University, Xi'an 710069, P.R. China
[b] Department of Chemistry and Chemical Engineering, Shangluo University, Shangluo 726000, P.R. China
Published online: 27 Sep 2011.

To cite this article: Fengying Chen, Zhenguo Jin, Hengxin Li & Shuiyang He (2011) Synthesis, crystal structure, and properties of two metal complexes of imidazole and an ONO donor hydrazone, Journal of Coordination Chemistry, 64:18, 3146-3157, DOI: 10.1080/00958972.2011.614948

To link to this article: http://dx.doi.org/10.1080/00958972.2011.614948

Journal of Coordination Chemistry
Vol. 64, No. 18, 20 September 2011, 3146–3157

Synthesis, crystal structure, and properties of two metal complexes of imidazole and an ONO donor hydrazone

FENGYING CHEN†‡, ZHENGUO JIN‡,
HENGXIN LI† and SHUIYANG HE*†

†College of Chemistry and Material Science, Shaanxi Key Laboratory of Physical-Inorganic Chemistry, Northwest University, Xi'an 710069, P.R. China
‡Department of Chemistry and Chemical Engineering, Shangluo University, Shangluo 726000, P.R. China

(*Received 17 May 2011; in final form 25 July 2011*)

Two complexes, $[Cd_2(Im)(HL)_2(CH_3OH)_3(H_2O)_2]$ (**1**) and $[Ni(HL)(Im)_2(H_2O)]\cdot[Ni(H_2L)(Im)_2(OH)]\cdot 4H_2O$ (**2**) (H_3L = N-(2-propionic acid)-salicyloyl hydrazone, Im = imidazole), have been synthesized and characterized by infrared and single-crystal X-ray diffraction. The bioactivity of **1** was studied by the turbidimetry/spectrometry method and DNA-binding properties of **2** were studied. The result showed that the inhibitory rate of **1** was very good and **2** binds to calf-thymus DNA by the groove-binding mode.

Keywords: Hydrazone; Imidazole; Crystal structure; DNA-binding

1. Introduction

Hydrazones are a versatile class of ligands with physiological and biological activities, used as insecticides, anticoagulants, antitumor agents, antioxidants, and plant growth regulators [1]. Complexes of hydrazones have contributed to the development of catalysis and enzymatic reactions, magnetism, molecular architectures, and materials chemistry [2, 3]. Complexes usually have better properties than the ligands or metal ions [4]. Imidazole is one of the biologically important ligands [5], monodentate at lower pH and at higher pH serves as a bridging ligand. The deprotonated form of imidazole is involved in the active site of bovine erythrocyte superoxide dismutase [6].

DNA-binding metal complexes have been extensively studied as DNA structural probes, DNA-dependent electron transfer probes, etc. [7–10]. The interaction of metal complexes, containing multidentate aromatic ligands, with DNA has important biological and medical roles [11, 12]. Studies of interaction between hydrazones and their metal complexes with DNA are important to further understand pharmacology of hydrazones [13–17]. The modes of DNA interaction with metal complex show intercalative behavior, electrostatic binding, and DNA cleavage ability [18, 19]. In this article, two complexes of N-(2-propionic acid)-salicyloyl hydrazone with imidazole

*Corresponding author. Email: xdchemistry411@126.com

ISSN 0095-8972 print/ISSN 1029-0389 online
DOI: 10.1080/00958972.2011.614948

as a co-ligand have been synthesized and characterized. The complexes interaction with calf-thymus DNA (CT-DNA) is examined by electronic absorption titration and viscosity.

2. Experimental

2.1. *Materials and physical measurements*

Pyruvic acid was a biochemical reagent; all other reagents were of AR grade. Infrared (IR) spectra were recorded on an EQUINOX 55 IR spectrophotometer using KBr pellets. The ultraviolet spectra were recorded on a Lambda 40P UV-Vis spectrophotometer. Fluorescence measurements were made on a Hitachi F-4500 spectrophotometer. The X-ray data for the crystals were collected on a Bruker Smart-1000 CCD X-ray single crystal diffractometer.

2.2. *Preparation*

2.2.1. Synthesis of H_3L [20]. Ligand H_3L was prepared by the following route:

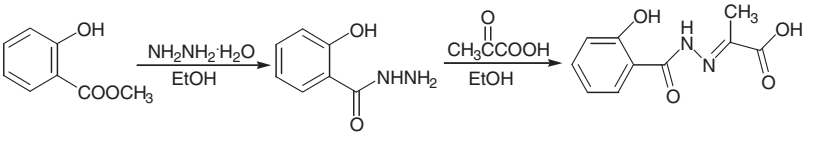

2.2.2. Synthesis of $[Cd_2(Im)(HL)_2(CH_3OH)_3(H_2O)_2]$ (1). A mixture of imidazole (4 mmol, 0.2724 g) and hydrazone (1 mmol, 0.2223 g) were dissolved in MeOH : H_2O=3 : 1 (40 mL, V/V) to obtain a yellow solution and a solution of $Cd(NO_3)_2 \cdot 4H_2O$ (1 mmol, 0.3085 g) in 10 mL water was added with continuous stirring. Then the mixture was refluxed for 2 h and filtered. After about 4 weeks at room temperature, brilliant yellow prism-shaped single crystals suitable for X-ray diffraction were obtained from the mother solution. Yield: 20%. IR (KBr pellet): 553, 754, 1379, 1459, 1559, 1602, 3145; Λ_m: 40.6 $\Omega^{-1} \cdot cm^2 \cdot mol^{-1}$.

2.2.3. Synthesis of $[Ni(HL)(Im)_2(H_2O)] \cdot [Ni(H_2L)(Im)_2(OH)] \cdot 4H_2O$ (2). Complex **2** was synthesized by a procedure similar to that of **1** using $Ni(Ac)_2 \cdot 4H_2O$ in place of $Cd(NO_3)_2 \cdot 4H_2O$. Yield: 26%. IR (KBr pellet): 558, 760, 1365, 1527, 1571, 1597, 3144; Λ_m: 43.0 $\Omega^{-1} \cdot cm^2 \cdot mol^{-1}$.

2.3. *X-ray crystal structure determination*

Data collections for **1** and **2** were performed at 293(2) K with graphite monochromated Mo-Kα radiation ($\lambda = 0.71073$ Å). The structures were solved by direct methods and

Table 1. Crystallographic information of **1** and **2**.

	1	**2**
Empirical formula	$C_{26}H_{36}Cd_2N_6O_{13}$	$C_{32}H_{44}N_{12}Ni_2O_{14}$
Formula weight	865.41	938.21
Wavelength (Å)	0.71073	0.71073
Crystal system	Triclinic	Monoclinic
Unit cell dimensions (Å, °)		
a	11.2535(11)	7.239(3)
b	12.4681(12)	19.606(7)
c	13.5117(13)	15.022(5)
α	98.128(2)	90
β	107.199(2)	95.139(5)
γ	110.192(2)	90
Volume (Å^3), Z	1635.9(3), 2	2123.5(13), 2
Calculated density (Mg m^{-3})	1.757	1.467
Absorption coefficient (mm^{-1})	1.372	0.963
$F(000)$	868	976
θ range for data collection (°)	1.64–25.10	1.36–25.00
Limiting indices	$-13 \le h \le 13$; $-14 \le k \le 11$; $-16 \le l \le 14$	$-7 \le h \le 8$; $-23 \le k \le 18$; $-17 \le l \le 17$
Reflections collected/unique	8329/5729 [R(int) = 0.0357]	10,697/5659 [R(int) = 0.1017]
Data/restraints/parameters	5729/7/459	5659/11/587
Goodness-of-fit on F^2	1.002	0.991
Final R indices [$I > 2\sigma(I)$]	$R_1 = 0.0456$, $wR_2 = 0.0859$	$R_1 = 0.0880$, $wR_2 = 0.2132$
R indices (all data)	$R_1 = 0.0947$, $wR_2 = 0.0949$	$R_1 = 0.1917$, $wR_2 = 0.2975$

refined by full-matrix least-squares on F^2 with the SHELXTL-97 program. Crystallographic information is summarized in table 1.

2.4. *Bioactivity experiment*

Coliform was used to test the bioactivities of **1** by turbidimetry/spectrometry method [21] and the growth curves of coliform as well as the inhibitor rate curves in the absence and presence of **1** were studied. The LB culture medium was prepared by mixing 2 g peptone, 1 g yeast, 1 g NaCl, and 200 mL H_2O. The experimental route was as follows: mixing 10 mL LB culture medium, 10 μL coliform solution, and 1 mL solution of **1** (0.25%) together, placing them on the rocking bed, cultivating at 37°C, measuring OD of each sample every 3 h, calculating inhibition rate, and drawing growth curves of coliform and inhibitor rate curves. The method is:

$$\text{Inhibitor rate (\%)} = \left[\text{OD}_{(\text{CK})} - \text{OD}_{(\text{sample})}\right]/\text{OD}_{(\text{CK})} \times 100\%.$$

Note: Here the CK sample is prepared by mixing 10 mL LB culture medium, 10 μL *coliform* solution, and 1 mL distilled water.

2.5. *Studies on DNA-binding mode*

Interactions of the complex with CT-DNA were carried out in a doubly distilled water buffer containing 5 mmol Tris, 0.4% DMSO, and 50 mmol NaCl and adjusted to pH 7.1 with hydrochloric acid. In order to eliminate the absorbance of nucleic acid itself, an

equal amount of CT-DNA was added into the sample and the reference cell, respectively. Spectrometric titrations were performed [22–24].

Viscosity experiments were conducted on an Ubbelodhe viscometer, immersed in a thermostated water-bath maintained at $25 \pm 0.1^{\circ}C$. Titrations were performed for the complexes ($10\,\mu mol\,L^{-1}$), and each compound was introduced into the CT-DNA solution ($10\,\mu mol\,L^{-1}$) present in the viscometer. Data were presented as $(\eta/\eta_0)^{1/3}$ *versus* the ratio of the concentration of the compound to CT-DNA, where η is the viscosity of CT-DNA in the presence of the compound and η_0 is the viscosity of CT-DNA alone. Viscosity values were calculated from the observed flow time of CT-DNA containing solutions corrected from the flow time of buffer alone (t_0), $\eta = t - t_0$ [25].

3. Results and discussion

3.1. *Structure descriptions*

Selected bond lengths and angles of the two complexes are given in tables 2 and 3. Hydrogen-bonding geometry is given in table 4. The crystal structure of **1** is shown in figure 1. The complex is neutral binuclear, consisting of two Cd ions connected by two μ2-bridging carboxyl oxygens, two tridentate ONO- donor hydrazones, two water molecules, three methanols, and an imidazole. Both cadmiums are seven-coordinate, however, with different coordination environments. Cd(1) is seven-coordinate *via* one

Table 2. Selected bond lengths (Å) and angles (°) of **1**.

Cd(1)–O(9)	2.272(5)	Cd(2)–N(5)	2.298(6)
Cd(1)–O(10)	2.309(5)	Cd(2)–O(13)	2.338(5)
Cd(1)–O(2)	2.344(4)	Cd(2)–O(4)	2.348(4)
Cd(1)–N(2)	2.360(5)	Cd(2)–O(12)	2.383(5)
Cd(1)–O(11)	2.363(5)	Cd(2)–O(6)	2.384(4)
Cd(1)–O(8)	2.371(4)	Cd(2)–N(3)	2.404(5)
Cd(1)–O(4)	2.425(4)	Cd(2)–O(8)	2.407(4)
O(9)–Cd(1)–O(10)	173.12(18)	N(5)–Cd(2)–O(4)	89.72(17)
O(9)–Cd(1)–O(2)	94.19(17)	O(13)–Cd(2)–O(4)	87.64(15)
O(10)–Cd(1)–O(2)	92.62(17)	N(5)–Cd(2)–O(12)	89.55(19)
O(9)–Cd(1)–N(2)	90.20(17)	O(13)–Cd(2)–O(12)	87.52(17)
O(10)–Cd(1)–N(2)	93.27(17)	O(4)–Cd(2)–O(12)	81.90(16)
O(2)–Cd(1)–N(2)	67.68(16)	N(5)–Cd(2)–O(6)	91.41(18)
O(9)–Cd(1)–O(11)	93.5(2)	O(13)–Cd(2)–O(6)	90.02(16)
O(10)–Cd(1)–O(11)	87.3(2)	O(4)–Cd(2)–O(6)	157.08(14)
O(2)–Cd(1)–O(11)	75.65(16)	O(12)–Cd(2)–O(6)	75.22(16)
N(2)–Cd(1)–O(11)	143.32(18)	N(5)–Cd(2)–N(3)	86.73(17)
O(9)–Cd(1)–O(8)	88.45(15)	O(13)–Cd(2)–N(3)	96.96(16)
O(10)–Cd(1)–O(8)	84.96(15)	O(4)–Cd(2)–N(3)	136.67(16)
O(2)–Cd(1)–O(8)	155.37(14)	O(12)–Cd(2)–N(3)	141.15(18)
N(2)–Cd(1)–O(8)	136.87(16)	O(6)–Cd(2)–N(3)	66.24(16)
O(11)–Cd(1)–O(8)	79.75(16)	N(5)–Cd(2)–O(8)	94.75(18)
O(9)–Cd(1)–O(4)	93.62(16)	O(13)–Cd(2)–O(8)	86.85(15)
O(10)–Cd(1)–O(4)	82.34(17)	O(4)–Cd(2)–O(8)	71.20(13)
O(2)–Cd(1)–O(4)	133.54(14)	O(12)–Cd(2)–O(8)	152.70(15)
N(2)–Cd(1)–O(4)	66.57(15)	O(6)–Cd(2)–O(8)	131.44(13)
O(11)–Cd(1)–O(4)	149.18(16)	N(3)–Cd(2)–O(8)	66.11(16)
O(8)–Cd(1)–O(4)	70.51(13)	N(5)–Cd(2)–O(13)	176.30(18)

Table 3. Selected bond lengths (Å) and angles (°) of **2**.

Ni(1)–N(2)	1.98(4)	Ni(2)–N(11)	2.03(4)
Ni(1)–N(3)	2.04(4)	Ni(2)–N(9)	2.06(5)
Ni(1)–O(2)	2.06(4)	Ni(2)–O(8)	2.10(4)
Ni(1)–O(4)	2.13(4)	Ni(2)–O(7)	2.12(4)
Ni(1)–N(5)	2.13(5)	Ni(2)–O(10)	2.17(4)
Ni(1)–O(5)	2.14(4)	Ni(2)–N(8)	1.98(5)
O(2)–Ni(1)–O(5)	89.4(15)	N(8)–Ni(2)–O(8)	77.4(17)
O(4)–Ni(1)–O(5)	88.7(15)	N(11)–Ni(2)–O(8)	101.9(15)
N(5)–Ni(1)–O(5)	178.5(17)	N(9)–Ni(2)–O(8)	90.9(17)
N(8)–Ni(2)–N(11)	176(2)	N(8)–Ni(2)–O(7)	77.8(17)
N(8)–Ni(2)–N(9)	91.9(19)	N(11)–Ni(2)–O(7)	102.9(15)
N(11)–Ni(2)–N(9)	92.0(19)	N(9)–Ni(2)–O(7)	90.6(17)
N(2)–Ni(1)–N(3)	177(2)	O(8)–Ni(2)–O(7)	155.1(13)
N(2)–Ni(1)–O(2)	79.4(16)	N(8)–Ni(2)–O(10)	89.2(17)
N(3)–Ni(1)–O(2)	99.8(16)	N(11)–Ni(2)–O(10)	86.9(18)
N(2)–Ni(1)–O(4)	78.9(15)	N(9)–Ni(2)–O(10)	178.1(17)
N(3)–Ni(1)–O(4)	101.8(15)	O(8)–Ni(2)–O(10)	87.8(14)
O(2)–Ni(1)–O(4)	158.2(14)	O(7)–Ni(2)–O(10)	91.1(15)
N(2)–Ni(1)–N(5)	91.4(19)	O(4)–Ni(1)–N(5)	92.4(17)
N(3)–Ni(1)–N(5)	91.7(19)	N(2)–Ni(1)–O(5)	89.7(15)
O(2)–Ni(1)–N(5)	89.9(17)	N(3)–Ni(1)–O(5)	87.1(16)

Table 4. Hydrogen-bonding geometry (Å, °) of **1** and **2**.

D–H···A	*d*(D–H)	*d*(H···A)	*d*(D···A)	∠(DHA)
Complex **1**				
O(1)–H(1)···N(1)	0.82	1.82	2.542(6)	146.4
O(5)–H(5A)···O(13)#1	0.82	2.49	2.751(7)	99.5
N(6)–H(6)···O(5)#2	0.86	2.08	2.881(8)	154.5
O(10)–H(27)···O(13)	0.814(10)	2.094(16)	2.897(7)	169(6)
O(12)–H(28)···O(3)	0.821(10)	1.877(13)	2.697(6)	178(11)
O(12)–H(28)···O(4)	0.821(10)	2.57(9)	3.101(6)	124(9)
O(11)–H(29)···O(7)	0.820(10)	1.824(18)	2.635(6)	169(8)
O(11)–H(29)···O(8)	0.820(10)	2.62(7)	3.035(7)	113(6)
O(9)–H(9D)···O(7)#3	0.818(10)	1.900(17)	2.707(6)	168(6)
O(9)–H(9E)···O(1)#4	0.818(10)	1.90(2)	2.698(6)	167(8)
O(13)–H(13A)···O(5)#1	0.821(10)	1.95(3)	2.751(7)	164(8)
O(13)–H(13B)···O(3)#5	0.818(10)	1.959(15)	2.768(6)	170(5)
Complex **2**				
N(4)–H(4A)···O(9)#6	0.86	1.97	2.83(5)	176.2
O(1)–H(1)···N(7)	0.82	2.68	3.45(7)	157.1
N(12)–H(12A)···O(3)#7	0.86	1.92	2.78(5)	175.7
N(12)–H(12A)···O(4)#7	0.86	2.63	3.18(6)	122.8
O(5)–H(5A)···O(3)#8	0.83	1.90	2.71(4)	168.4
N(1)–H(1A)···O(1)	0.86	1.89	2.55(6)	132.6
N(6)–H(6A)···O(7)#9	0.86	2.31	3.16(7)	171.9
O(14)–H(14A)···O(11)#10	0.83(6)	2.22(17)	3.02(10)	161(38)
O(11)–H(11B)···O(13)#11	0.85(18)	2.3(5)	2.90(9)	126(57)
O(13)–H(13A)···O(8)	0.82(4)	2.2(3)	2.89(7)	149(54)
O(13)–H(13A)···O(10)	0.82(4)	2.6(4)	3.13(7)	123(46)
O(13)–H(13B)···O(14)#12	0.82(6)	2.4(5)	2.73(11)	107(38)
O(10)–H(10B)···O(1)	0.84(5)	2.2(3)	2.87(6)	142(32)
O(10)–H(10B)···N(8)	0.84(5)	2.4(3)	2.92(6)	120(29)
O(10)–H(10B)···O(1)	0.84(5)	2.2(3)	2.87(6)	142(32)

Symmetry transformations used to generate equivalent atoms: #1 $-x+1, -y+1, -z+2$; #2 $-x+2, -y+1, -z+2$; #3 $-x+2, -y+2, -z+2$; #4 $-x+2, -y+2, -z+1$; #5 $-x+1, -y+1, -z+1$; #6 $x, y, z+1$; #7 $x, y, z-1$; #8 $x+1, y, z$; #9 $-x, y-1/2, -z+1$; #10 $-x+1, y-1/2, -z+1$; #11 $-x+1, y+1/2, -z+1$; #12 $x-1, y, z$.

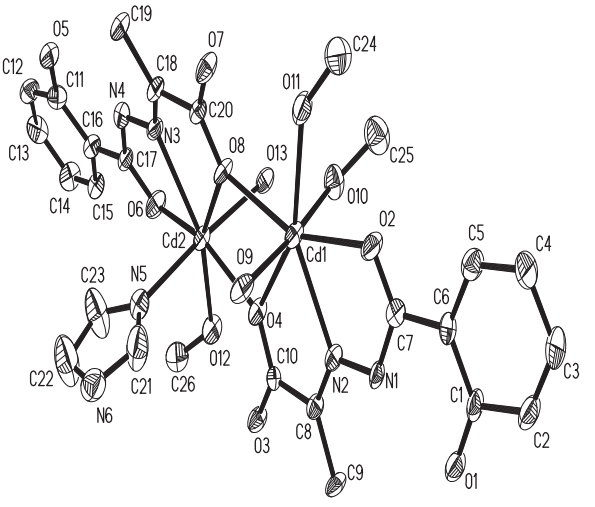

Figure 1. ORTEP diagram of **1**.

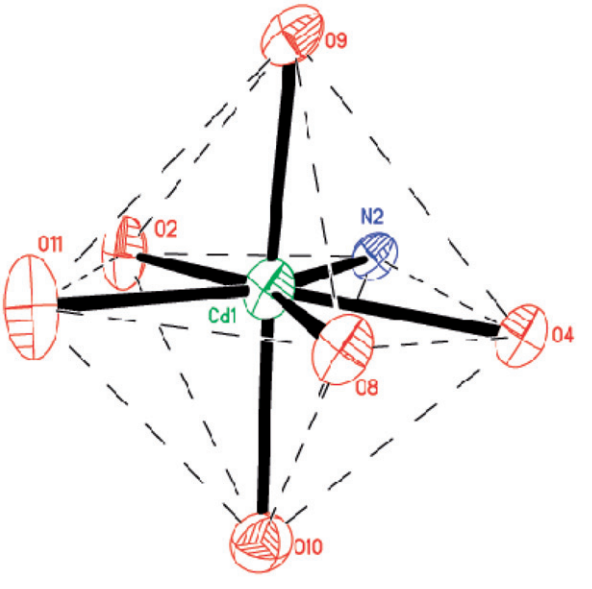

Figure 2. Coordination environment around the Cd(1).

water molecule, one tridentate HL^{2-} and two methanols, while Cd(2) is coordinated by one water molecule, one tridentate HL^{2-}, one methanol, and one imidazole. The coordination polyhedra can be described as distorted pentagonal bipyramids (figure 2). O(2), N(2), O(4), O(8), and O(11) are approximately coplanar for Cd(1) and form the equatorial plane; O(9) and O(10) occupy axial sites with bond angle O(9)–Cd(1)–O(10) being 173.14°. For Cd(2), O(4), N(3), O(6), O(8), and O(12) form the equatorial plane; O(13) and N(5) occupy the axial sites. There are abundant hydrogen bonds in **1** (figure 3). Intramolecular hydrogen bonds are formed by nitrogen and oxygen of the

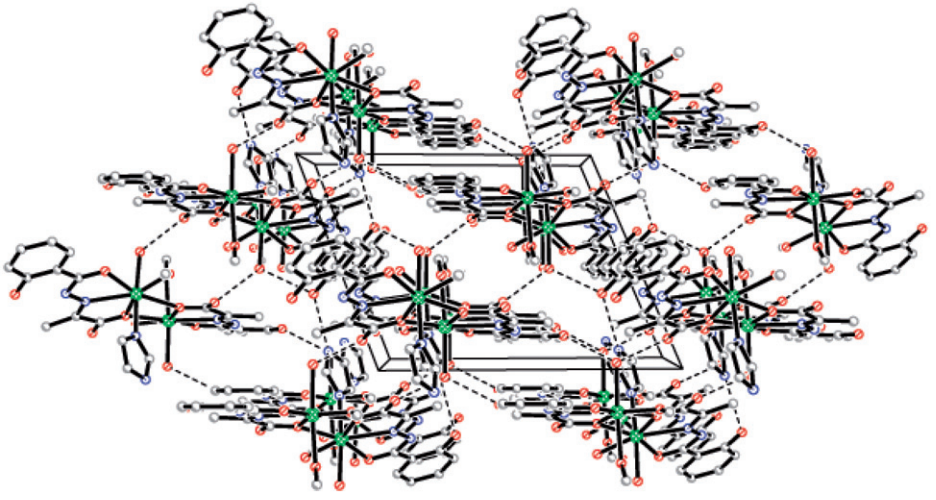

Figure 3. Packing diagram of **1**, hydrogens are omitted for clarity.

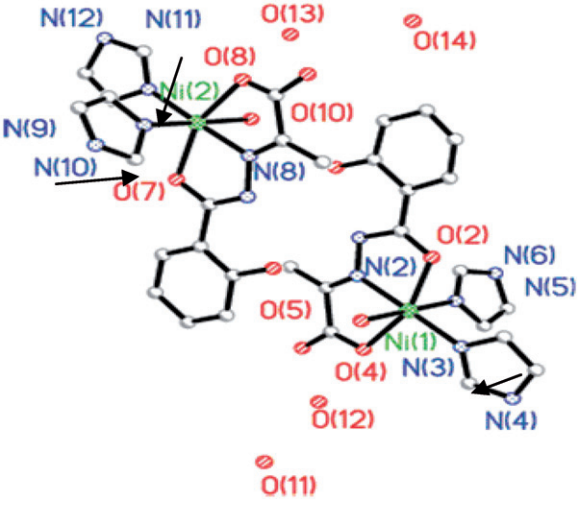

Figure 4. ORTEP diagram of **2**.

ONO-donor hydrazones, methanol, and water, such as O(1)–H(1)···N(1), O(10)–H(27)···O(13), O(12)–H(28)···O(3), O(12)–H(28)···O(4), O(11)–H(29)···O(7), and O(11)–H(29)···O(8). Intermolecular hydrogen bonds exist between imidazole, coordinated water, methanol, and hydrazones. These inter- and intra-molecular hydrogen bonds (O–H···N and O–H···O) give rise to the 3-D network.

The crystal structure of **2** consists of one $[Ni(C_{10}H_8N_2O_4)(C_3H_4N_2)_2(H_2O)]$, one $[Ni(C_{10}H_9N_2O_4)(C_3H_4N_2)_2(OH)]$, and four lattice water molecules. Coordination geometry around nickel(II) is a distorted octahedron. Ni1 is six-coordinate composed of three nitrogen atoms (N2 of hydrazone and N3, N5 of different imidazoles) with three different oxygen atoms, two (O2, O4) from a hydrazone and one (O5) from a water molecule (figure 4). Due to the MA_3B_3 framework (where M is metal, A and B

are different coordinated atoms), it can adopt facial (*fac*-) and meridional (*mer*-) isomers. In this instance, the complex is meridional in the solid state. Selected bond lengths and angles are shown in table 2. The Ni1–N2 distance is 1.971(13) Å and the distance to the imidazole donors N3 and N5 are 2.023(14) and 2.080(16) Å, respectively. Owing to chelation strain, the bond distances Ni1–N2 and Ni2–N8 are shorter than those of imidazole donors. The Ni1–O5 distance is 2.163(12) Å and the distances to hydrazone O2 and O4 are 2.109(12) and 2.132(13) Å. The average Ni–N bond length is 2.025 Å while the average Ni–O bond length is 2.135 Å. The bond angles N(2)–Ni(1)–O(2) (79.4(16)°), N(2)–Ni(1)–O(4) (78.9(15)°), N(3)–Ni(1)–O(4) (101.8(15)°), and N(3)–Ni(1)–O(2) (99.8(16)°) sum up to 360° and the angle N(5)–Ni(1)–O(5) (178.5(17)°) is approximately 180°, so the coordinated geometry of Ni1 may be described as distorted octahedron with Ni1, O2, N2, O4, and N3 forming the equatorial plane and N5, O5 occupying the axial positions (figure 5). The dihedral angle between the plane (Ni1, O2, O4, N2, and N3) and the plane (O5, Ni1, N5) is 88.95°.

There are intramolecular and intermolecular hydrogen-bond interactions (table 4), intramolecular interaction between the phenolic oxygen (O1, O6), and imine nitrogen (N1, N7) (N(1)–H(1 A)···O(1) 2.517(17) with bond angle 132.9°, N(7)–H(7)···O(6) 2.514(17) with bond angle 130.9°). Intermolecular hydrogen-bond interactions are of three types: between lattice water oxygen atoms (O(12)–H(12 A)···O(13) 2.77(3)), between water oxygen and imidazole nitrogen (N(10)–H(12 C)···O(12) 2.96(3)) and between imidazole nitrogen and carboxylic oxygen atoms (N(12)–H(10 C)···O(3) 3.198(19), N(12)–H(10C)···O(4) 2.819(17)), and the last is between water and carboxylic oxygen atoms (O(10)–H(10B)···O(9) 2.742(15)). The hydrogen bonds N(4)–H(5C)···O(9), N(12)–H(10C)···O(3), O(1)–H(1)···O(10) and O(5)–H(5A)···O(6) link the molecules to infinite 1-D chains (figure 6). The lattice water molecules act as a hydrogen bond donor/acceptor to form several hydrogen bonds.

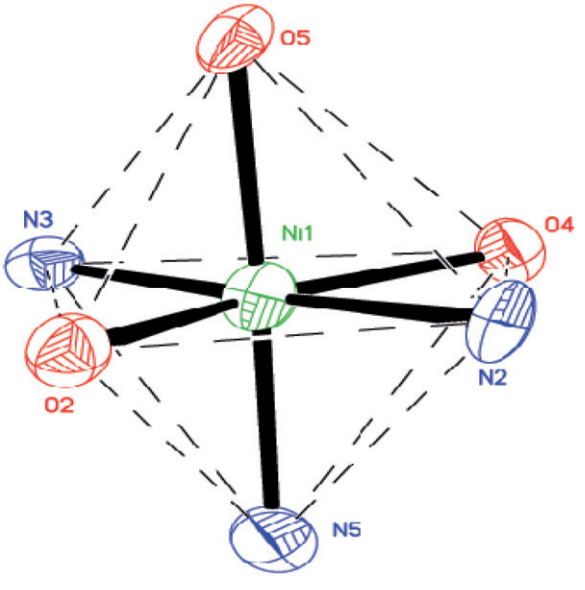

Figure 5. Coordination environment around the Ni(1).

3.2. *Bioactivity experiment*

Complex **1** was selected to test the bioactivity against *coliform* and the growth curves of coliform, and the inhibitor rate curves in the absence and presence of complex are shown in figure 7(a) and (b), respectively. The curves in figure 7(a) showed that the growth speed of coliform was much slower with the presence of **1**. That is to say, the complex can inhibit the growth of *coliform*. The inhibitory rate curve of the compound is shown in figure 7(b). During 0–4 h, the inhibitory rate increased quickly, and then the speed increased slowly at 4–8 h. The antimicrobial effect of complex reached 80.3%. Although the inhibitor rate is not very good and the mechanisms of antimicrobial action of the compound still need further investigation, the assay results provide basic data for the pharmacological research of these types of compounds.

3.3. *DNA-binding study*

The application of electronic absorption spectroscopy in DNA-binding studies is one of the most useful techniques [26, 27]. The absorption spectra of **2** in the absence and presence of DNA are shown in figure 8. The addition of DNA to solutions of the

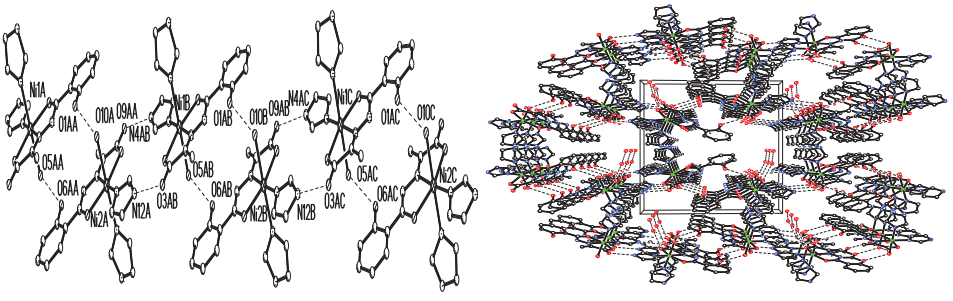

Figure 6. Packing diagram of **2**.

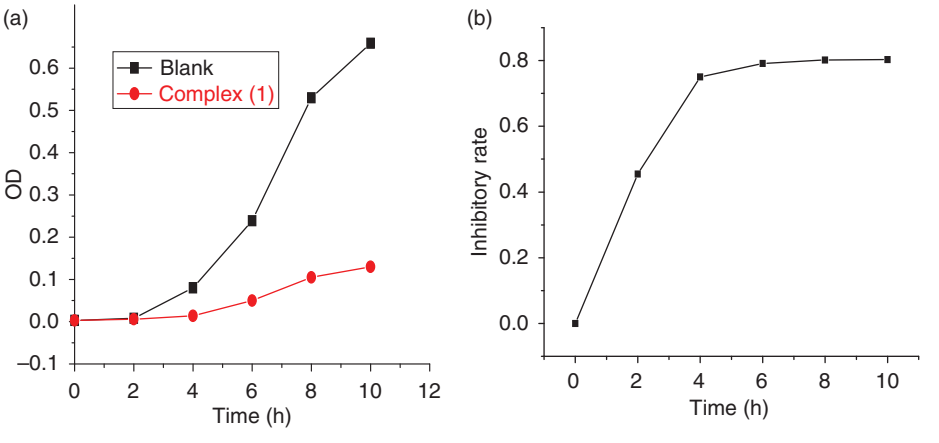

Figure 7. (a) Growth curves of coliform and (b) inhibitor rate curves of **1**.

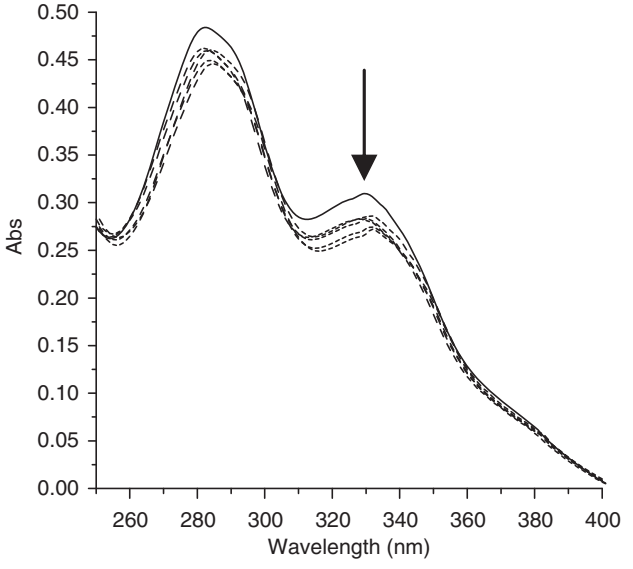

Figure 8. Electronic spectra of **2** in the absence (—) and presence (···) of CT-DNA. Arrow shows the absorbance changes upon increasing DNA concentration.

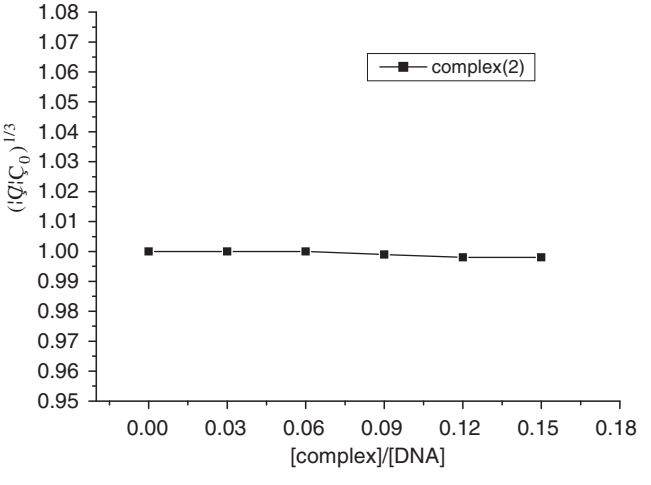

Figure 9. Effect of complexes on the viscosity of CT-DNA.

complex induces hypochromic responses of about 7.87% and 12.07% at 282 and 330 nm, but there are no evident red shifts. These spectral variations of the complex may be considered as characteristic of aromatic chromophore (π–π^*) interactions with the nucleic acid bases [28]. As reported previously [29], a change in band intensity upon the addition of DNA to metal complexes implies interaction of the complexes with DNA base pairs. For **1**, there are no red shifts observed, so it seems that the complex binds to DNA by groove binding [30].

To clarify further the interaction of the complex and CT-DNA, viscosity measurements were carried out (figure 9). In classical intercalation, the DNA helix lengthens as

base pairs are separated to accommodate the bound ligand leading to increased DNA viscosity [31], whereas in groove binding or electrostatic mode the length of the helix is unchanged resulting in no alteration in DNA viscosity [32]. In this case, addition of **2** to aqueous CT-DNA solutions resulted in very slight lowering of relative viscosities. Such observations are consistent with substrates that bind to DNA through groove binding [33].

4. Conclusion

Two transition metal complexes have been synthesized and characterized. The bioactivity of **1** against *coliform* was tested by the turbidimetry/spectrometry method; the results show that **1** has good antibacterial activity against *coliform*. The DNA-binding properties of **2** were studied by electronic absorption spectroscopy and viscosity. The results indicted that it binds to DNA by groove binding.

Acknowledgments

This study was supported by the program of technological plan of Xi'an (NC09052) and Education committee of Shaanxi Province (No. 08JK279).

References

[1] Y.P. Kitaev, B.I. Buzykin, T.V. Troepolskaya. *Russ. Chem. Rev.*, **39**, 441 (1970).
[2] R.A. Archer. *Coord. Chem. Rev.*, **128**, 49 (1993).
[3] T. Kaliyappan, P. Kannan. *Prog. Polym. Sci.*, **25**, 343 (2000).
[4] I.M. Gabr. *J. Coord. Chem.*, **62**, 3206 (2009).
[5] R.N. Patel, Nripendra Singh, V.L.N. Gundla. *Polyhedron*, **25**, 3312 (2006).
[6] R.N. Patel, Nripendra Singh, K.K. Shukla, U.K. Chauhan. *Spectrochim. Acta*, **61**, 287 (2005).
[7] B.Y. Wu, L.H. Gao, Z.M. Duan, K.Z. Wang. *J. Inorg. Biochem.*, **99**, 1685 (2005).
[8] K.E. Erkkila, D.T. Odom, J.K. Barton. *Chem. Rev.*, **99**, 2777 (1999).
[9] C. Metcalfe, J.A. Thomas. *Chem. Soc. Rev.*, **32**, 215 (2003).
[10] A. Silvestri, G. Barone, G. Ruisi, M.T. Lo Giudice, S. Tumminello. *J. Inorg. Biochem.*, **98**, 589 (2004).
[11] Z.Y. Yang, B.D. Wang, Y.H. Li. *J. Org. Met. Chem.*, **691**, 4159 (2006).
[12] B.D. Wang, Z.Y. Yang, T.R. Li. *Bioorg. Med. Chem.*, **14**, 6012 (2006).
[13] C. Hemmert, M. Pitié, M. Renz, H. Gornitzka, S. Soulet, B. Meunier. *J. Biol. Inorg. Chem.*, **6**, 14 (2001).
[14] Y. Wang, Y. Wang, Z.Y. Yang. *Spectrochim. Acta A*, **66**, 329 (2007).
[15] B.D. Wang, Z.Y. Yang, T.R. Li. *Bioorg. Med. Chem.*, **14**, 6012 (2006).
[16] B.D. Wang, Z.Y. Yang, Q. Wang, T.K. Cai, P. Crewdson. *Bioorg. Med. Chem.*, **14**, 1880 (2006).
[17] S. Srinivasan, J. Annaraj, P.R. Athappan. *J. Inorg. Biochem.*, **99**, 876 (2005).
[18] P.J. Cox, G. Psomas, C.A. Bolos. *Bioorg. Med. Chem.*, **17**, 6054 (2009).
[19] G. Barone, N. Cambino, A. Ruggirello, A. Silvestri, A. Terenzi, V.T. Liveri. *J. Inorg. Biochem.*, **103**, 731 (2009).
[20] S.Y. He, Y. Liu, J.S. Zhao, H.A. Zhao, R. Yang, R.Z. Hu, Q.Z. Shi. *Chin. J. Chem.*, **21**, 139 (2003).
[21] F.Y. Chen, S.Y. He. *Synth React. Inorg. Met.-Org. Chem.*, **38**, 642 (2008).
[22] S. Satyanarayana, J.C. Dabrowiak, J.B. Chaires. *Biochemistry*, **31**, 9319 (1992).
[23] Y. Wang, Z.Y. Yang. *Transition Met. Chem.*, **30**, 902 (2005).
[24] H.B. Li, X.M. Wang, H.P. Liu, Y.M. Hu, D.M. Yang, R.M. Shi, F.Q. Dong. *Chin. J. Inorg. Chem.*, **22**, 1695 (2006).
[25] M.T. Carter, M. Rodriguez, A.J. Bard. *J. Am. Chem. Soc.*, **111**, 8901 (1989).

[26] J.K. Barton, A. Danishefsky, J. Goldberg. *J. Am. Chem. Soc*., **106**, 2172 (1984).
[27] T.M. Kelly, A.B. Tossi, D.J. McConnell, T.C. Strekas. *Nucleic Acids Res*., **13**, 6017 (1985).
[28] S.A. Tysoe, R.J. Morgan, A.D. Baker, T.C. Strekas. *J. Phys. Chem*., **97**, 1707 (1993).
[29] H.P. Yang, W.H. Zhang, Q.X. Zhao, J.Y. Cai. *Chin. J. Inorg. Chem*., **22**, 488 (2006).
[30] R.C. Yadav, G.S. Kumar, K. Giri, P. Bhadra, R. Pal, S. Sinha, M. Maiti. *Bioorg. Med. Chem*., **13**, 165 (2005).
[31] S. Satyanarayana, J.C. Dabrowiak, J.B. Chaires. *Biochemistry*, **32**, 2573 (1993).
[32] S. Satyanarayana, J.C. Dabrowiak, J.B. Chaires. *Biochemistry*, **31**, 9319 (1992).
[33] C. Metcalfe, C. Rajput, J.A. Thomas. *J. Inorg. Biochem*., **100**, 1314 (2006).